

A MONTE CARLO APPROACH TO MAGNETAR-POWERED TRANSIENTS: I. HYDROGEN-DEFICIENT SUPERLUMINOUS SUPERNOVAE

LIANG-DUAN LIU^{1,2}, SHAN-QIN WANG^{1,2,3}, LING-JUN WANG⁴, ZI-GAO DAI^{1,2}, HAI YU^{1,2}, ZONG-KAI PENG^{1,2}

¹School of Astronomy and Space Science, Nanjing University, Nanjing 210093, China; dzg@nju.edu.cn

²Key Laboratory of Modern Astronomy and Astrophysics (Nanjing University), Ministry of Education, China

³Department of Astronomy, University of California, Berkeley, CA 94720-3411, USA and

⁴Key Laboratory of Space Astronomy and Technology, National Astronomical Observatories, Chinese Academy of Sciences, Beijing 100012, China

Draft version September 28, 2018

ABSTRACT

In this paper we collect 19 hydrogen-deficient superluminous supernovae (SLSNe) and fit their light curves, temperature evolution, and velocity evolution based on the magnetar-powered model. To obtain the best-fitting parameters, we incorporate the Markov Chain Monte Carlo approach. We get rather good fits for 7 events ($\chi^2/\text{d.o.f} = 0.24 - 0.96$) and good fits for other 7 events ($\chi^2/\text{d.o.f} = 1.37 - 3.13$). We find that the initial periods (P_0) and magnetic strength (B_p) of the magnetars supposed to power these SLSNe are in the range of $\sim 1.2 - 8.3$ ms and $\sim (0.2 - 8.8) \times 10^{14}$ G, respectively; the inferred masses of the ejecta of these SLSNe are between 1 and $27.6 M_\odot$, and the values of the gamma-ray opacity κ_γ are between 0.01 and $0.82 \text{ cm}^2 \text{ g}^{-1}$. We also calculate the fraction of the initial rotational energy of the magnetars harbored in the centers of the remnants of these SLSNe that is converted to the kinetic energy of the ejecta and find that the fraction is $\sim 19 - 97\%$ for different values of P_0 and B_p , indicating that the acceleration effect cannot be neglected. Moreover, we find that the initial kinetic energies of most of these SLSNe are so small ($\lesssim 2 \times 10^{51}$ erg) that they can be easily explained by the neutrino-driven mechanism. These results can help clarify some important issues related to the energy-source mechanisms and explosion mechanisms and reveal the nature of SLSNe.

Subject headings: stars: magnetars – supernovae: general

1. INTRODUCTION

Superluminous supernovae (SLSNe; Quimby et al. 2011; Gal-Yam 2012), whose peak luminosities are $\gtrsim 10^{44} \text{ erg s}^{-1}$, have been discovered and studied in the last decade. According to their optical spectra near maximum light, SLSNe can be divided into types I (hydrogen-deficient) and II (hydrogen-rich); the detailed classification schemes of SNe based on their spectra were summarized by Filippenko 1997 and Gal-Yam 2016). To date, all SLSNe-I are type Ic SNe whose spectral features resemble that of the normal-luminosity SNe Ic (Pastorello et al. 2010; Gal-Yam 2012; Inserra et al. 2013; Nicholl et al. 2016b). While most SLSNe-II have narrow H α emission lines in their optical spectra and can be regarded as the high-luminosity versions of normal SNe IIn, a few SLSNe II do not have H α emission lines and their spectra resemble those of SNe IIL (Gezari et al. 2009; Miller et al. 2009; Inserra et al. 2016).

The problems of the origin of the energy sources and explosion mechanisms of SLSNe have not yet been completely solved. Currently, the most prevailing energy-source models explaining SLSNe are magnetar-powered model (e.g., Kasen & Bildsten 2010; Woosley 2010; Dessart et al. 2012; Inserra et al. 2013; Chen et al. 2015; Wang et al. 2015a, 2016c; Dai et al. 2016; Wang et al. 2016d)¹, the ejecta-circumstellar medium (CSM) interaction model (Chevalier 1982; Chevalier & Fransson

1994; Chugai & Danziger 1994; Chugai 2009; Chevalier & Irwin 2011; Chatzopoulos et al. 2012; Ginzburg & Balberg 2012), and the pair instability supernova (PISN) model (Barkat et al. 1967; Rakavy & Shaviv 1967) which is essentially ⁵⁶Ni-powered (Colgate & McKee 1969; Colgate et al. 1980; Arnett 1982) but requires a huge amount ($\gtrsim 5M_\odot$) of ⁵⁶Ni. Some SLSNe show double-peaked light curves (Nicholl et al. 2015a; Nicholl & Smartt 2016; Smith et al. 2016; Vreeswijk et al. 2017) and their early-time excess emission might be due to the cooling emission from shock-heated envelopes of the progenitors while the main peaks can be explained by the magnetar-powered model or interaction model.

Determining the energy-source models for SLSNe is rather tricky. For example, Gal-Yam et al. (2009) proposed that SN 2007bi, whose light-curve decline rate is approximately equal to the decay rate of ⁵⁶Co, is a PISN, but Dessart et al. (2012) argued that it might not be a PISN since its spectrum is inconsistent with the spectrum produced by the PISN model; Nicholl et al. (2013) demonstrated that another slow declining SLSN PTF12dam, whose post-peak light curve mimics that reproduced by the PISN model, is not yet a PISN since the rising part of its light curve cannot be explained by the PISN model.

Except for the two high-redshift SLSNe (SN 2213-1745 and SN 1000+0216) that are believed to be PISNe (Cooke et al. 2012) and SN 2007bi whose explosion

¹ It has long been recognized that the dipole radiation from the nascent neutron stars can enhance the luminosities of the normal SNe (Ostriker & Gunn 1971; Maeda et al. 2007).

mechanism is still in debate,² all SLSNe discovered cannot be explained by the PISN model since the ratio of required masses of ^{56}Ni to inferred ejecta masses are too large and/or the theoretical light curves did not fit the observational data (Quimby et al. 2011; Inserra et al. 2013; Nicholl et al. 2013, 2014). This fact in turn indicates that most SLSNe observed might be core-collapse SNe (CCSNe) since the peak luminosities of type Ia SNe cannot reach 10^{44} erg s $^{-1}$.³

SLSNe that cannot be explained by PISN model can be explained by the magnetar-powered model (Inserra et al. 2013; Nicholl et al. 2013, 2014) or the ejecta-CSM interaction model (e.g. Smith & McCray 2007; Moriya et al. 2013; Nicholl et al. 2014). The magnetar-powered model proposes that the nascent neutron stars with initial rotational periods of a few milliseconds and magnetic strength of $10^{13} - 10^{15}$ G inject their rotational energy to the ejecta of SNe, while the ejecta-CSM interaction model supposes that the interaction between the SN ejecta and the CSM surrounding the progenitors of the SNe can release a huge amount of energy and heat the SN ejecta. These two processes can significantly enhance the luminosities of the SNe and lead them to be SLSNe.

In this paper we focus on the SLSNe that were demonstrated not to be PISNe. While the ejecta-CSM model cannot be excluded in explaining these SLSNe Ic, we do not adopt it due to the absence of the interaction signatures (e.g., narrow $\text{H}\alpha$ emission lines) that are indicative of strong interaction between the ejecta and CSM. Studies have shown that the magnetar-powered model can well reproduce the light curves of these SLSNe, and indicated that the magnetar-powered model has special advantages since it does not need ad hoc assumptions about the pre-supernova mass-loss history. Therefore, the magnetar model is preferred in modeling SLSNe Ic.

Most previous studies using the magnetar-powered model focused on the light-curve fitting. Some group fitted the light curves, temperature evolution and the evolution of photospheric radii of SLSNe. However, the photospheric radius of an SLSN cannot be measured directly, and it is derived from the luminosity and temperature ($L = 4\pi\sigma T^4 R^2$, where L is the luminosity, σ is the Stefan-Boltzman constant, T is the temperature, and R is the photospheric radius).

In this paper, we collect a sample of 19 type I SLSNe and use the magnetar-powered model proposed by Wang et al. (2016c) to fit their light curves, temperature evolution, and velocity evolution. To obtain the best-fitting parameters, we use the Markov Chain Monte Carlo (MCMC) code developed by Wang et al. (2017b), who employed this approach (magnetar-powered model + MCMC) to fit the light curves of SNe 1998bw and

² Inserra et al. (2017) assembled four low-redshift slow-evolving SLSNe I (SN 2007bi, PTF12dam, SN 2015bn, and LSQ14an) and found the declines of their light curves at $t - t_{\text{peak}} \gtrsim 150$ days are faster than ^{56}Co and further steepen after 300 days, which indicates that these four SLSNe I cannot be explained by the PISN model since the required ejecta are so massive that the decline rates of the light curves must be consistent with that of ^{56}Co decay at $t - t_{\text{peak}} \gtrsim 500$ days. A similar analysis cannot be performed for high-redshift analogues since the lower quality late-time data prevent further investigation, and therefore the possibility that high-redshift slow-evolving SLSNe are PISNe cannot be excluded.

³ Type Ia SNe magnified by the gravitational lensing effect, e.g., PS1-10afx (Quimby et al. 2013, 2014), are not genuine SLSNe.

2002ap.

This paper is organized as follows. In Section 2, we present our sample and describe the magnetar-powered model adopted. In Section 3, we use the magnetar-powered model and the MCMC code to get the best-fitting parameters. We discuss implications of our results in Section 4 and give some conclusions in Section 5. In our another paper (Wang et al. 2017a), we systematically study the whole sample of broad-lined type Ic supernovae not associated with gamma-ray bursts. We find that the magnetar-powered model can also well account for both the light curves and velocity evolution of these SNe.

2. SAMPLING AND MODELING

We collect 19 type I (Ic) SLSNe in the literature, see Table 1. All of these SLSNe have light curves and temperature data, and most of them have velocity data. These SLSNe are selected because the observational errors were provided by the original papers so that we can run the MCMC code against them.

The most prevailing magnetar model are the model proposed by Chatzopoulos et al. (2012) and Inserra et al. (2013) the model revised by Wang et al. (2015a) and Chen et al. (2015) by incorporating the hard emission leakage effect. These semi-analytical magnetar-powered models used to fit most type I SLSNe neglect the photospheric recession effect and acceleration of the SN ejecta caused by the magnetar wind. Kasen & Bildsten (2010) and Woosley (2010) proposed the magnetar-powered model for SLSNe and demonstrated the acceleration effect is rather notable but they do not take into account the leakage effect. Wang et al. (2016c) proposed a revised magnetar model that took into account all these effects (leakage effect, photospheric recession effect and acceleration effect). So we use this revised magnetar-powered model to fit the observed data.

In this revised magnetar-powered model, the photospheric velocities of SLSNe cannot be fixed to be their scale velocities v_{sc} and their evolution must be fitted. Moreover, the scale velocity itself is a varying quantity and not directly measurable. Instead, the initial scale velocity $v_{\text{sc}0}$ is a free parameter. If the neutrinos emitted from proto-neutron stars provide the initial kinetic energy (KE) and initial velocity, then the values of $v_{\text{sc}0}$ must have a lower limit to ensure that the initial KE of SNe can be larger than the lower limit of the initial KE provided by neutrinos ($\sim 10^{50}$ erg, Janka et al. 2016, and references therein).

Other parameters in this model include the mass of ejecta M_{ej} , grey optical opacity κ , magnetic strength of magnetar B_p , initial rotational period of the magnetar P_0 , and the gamma-ray opacity κ_γ to magnetar photons.⁴ Here the subscript “ p ” in B_p means the surface dipole magnetic field of the magnetar (Shapiro & Teukolsky 1983). The optical opacity κ is somewhat uncertain and we adopt the value $0.1 \text{ cm}^2 \text{ g}^{-1}$ throughout this paper. Because the explosion time of an SLSN is not an ob-

⁴ In order to quantitatively describe the leakage effect associated with gamma and X-ray photons emitted from the magnetar, Wang et al. (2015a) incorporated the trapping factor $(1 - e^{-At^{-2}})$ into the original magnetar-powered model, $A = 3\kappa_\gamma M_{\text{ej}}/4\pi v^2$, κ_γ is the effective gamma ray opacity.

servable quantity, a free parameter T_{start} is included to refer to the theoretical explosion time relative to the zero epoch given in the paper from which the observed data have been taken. In the papers providing the data, sometimes the zero epochs refer to the peak times, and otherwise the zero epochs refer to the inferred explosion times.

While the PISN model (pure ^{56}Ni -powered model) has been excluded by previous studies for most type I SLSNe, a moderate amount of ^{56}Ni synthesized by these SLSNe cannot be completely neglected. However, the masses of ^{56}Ni synthesized by CCSNe are usually only $0.04 - 0.2M_{\odot}$ for normal CCSNe and $0.2 - 0.5M_{\odot}$ (see e.g., Figure 8 of [Mazzali et al. 2013](#)) for some Hypernovae whose kinetic energies were inferred to be $\gtrsim 10^{52}$ erg.⁵ When we study an SLSNe whose peak luminosities $\gtrsim 10^{44}$ erg s $^{-1}$, the contribution of $0.1 - 0.5M_{\odot}$ of ^{56}Ni is significantly lower than the contribution from magnetars or the ejecta-CSM interaction and can therefore be neglected (e.g., [Inserra et al. 2013](#); [Chen et al. 2015](#)) since $0.1 - 0.5M_{\odot}$ of ^{56}Ni will power a peak luminosity of $\sim 2 \times 10^{42} - 1 \times 10^{43}$ erg s $^{-1}$ if the rise time is ~ 18 days and a lower peak luminosity for longer rise time.⁶

Hence, we neglect the contribution from ^{56}Ni in our modeling, i.e., the mass of ^{56}Ni is set to be zero. In summary, the free parameters in this model are M_{ej} , B_p , P_0 , $v_{\text{sc}0}$, κ_{γ} , and T_{start} . To get the best-fitting parameters and estimate the uncertainties of the parameters, we use the code developed by [Wang et al. \(2017b\)](#) who incorporated MCMC approach into our revised magnetar-powered model.

3. RESULTS

Using the magnetar-powered model and the MCMC approach, we find that the light curves, temperature evolution, and velocity evolution reproduced by the model are in excellent agreement with the observational data of LSQ14mo, PS1-10awh, PS1-10bzj, SN 2010gx, SN 2011kf, and PS1-11ap, see Figure 1. The light curves and temperature data of SN 2012il, PTF12dam, PTF11rks, SN 2013dg, SSS120810, PTF10hgi, Gaia16apd, and DES13S2cmm can also be explained by the model, but the velocities reproduced by the model are larger or smaller than the data of these SLSNe, see Figure 2. DES13S2cmm is also in this group since it do not have velocity data. The light curves of SN 2011ke, SN 2015bn, LSQ12dlf, DES14X3taz, and PS1-14bj can also be well reproduced by the model, but both the temperature evolution and velocity evolution of these SLSNe do not fit the theoretical curves well, see Figure 3. In these figures, the zero epochs all refer to the peak times of the SLSN light curves.

The best-fitting parameters as well as the values of $\chi^2/\text{d.o.f}$ are listed in Table 2 and their error bars can be appreciated by inspecting Figure 4. Some parameters, e.g., κ_{γ} and $v_{\text{sc}0}$ of some SNe (see Figure 4), cannot be tightly constrained and therefore only their 1σ upper limits or lower limits are presented in this table.

⁵ There is evidence that at least some hypernovae were powered by magnetars ([Wang et al. 2017b](#)) and the required ^{56}Ni mass and initial explosion energy are significantly smaller than previously believed ([Wang et al. 2016b, 2017a](#)).

⁶ For the luminous SNe whose peak luminosity $\sim 5 \times 10^{43}$ erg s $^{-1}$, the contribution from ^{56}Ni cannot be neglected ([Wang et al. 2015b](#)).

From Table 2, we find that the magnetars' initial periods and the magnetic field strengths are $1.2 - 8.3$ ms and $0.2 - 8.8 \times 10^{14}$ G, respectively, consistent with theoretical expectation and the results of previous modelings. The gamma-ray opacity κ_{γ} directly determining the magnitude of late-time leakage effect is between 0.01 and $0.8 \text{ cm}^2 \text{ g}^{-1}$. Assuming that $\kappa = 0.1 \text{ cm}^2 \text{ g}^{-1}$, the masses of these SLSNe are between $1 - 27.6M_{\odot}$. [Nicholl et al. \(2015b\)](#) have fitted the light curves of 24 hydrogen-deficient SLSNe and found that the range of their ejecta masses is $3 - 30M_{\odot}$ if $\kappa = 0.1 \text{ cm}^2 \text{ g}^{-1}$. Both the lower limit and the upper limit of the mass range in our sample are smaller than the values inferred by [Nicholl et al. \(2015b\)](#). If we adopt a larger κ , e.g., $0.2 \text{ cm}^2 \text{ g}^{-1}$, the ejecta mass must be halved. Although the acceleration effect must be obvious for less massive ejecta, the light curves have only a slight change, i.e., the degeneracy between the κ and M_{ej} would not be broken.

The initial scale velocity $v_{\text{sc}0}$ of the ejecta of these SLSNe is between $\sim 1,100 \text{ km s}^{-1}$ and $1.7 \times 10^4 \text{ km s}^{-1}$. Based on the values of M_{ej} and $v_{\text{sc}0}$, the initial KE $E_{\text{K}0}$ of these SLSNe can be calculated. In the beginning of the expansion when the acceleration does not take place, the initial KE can be calculated according to $E_{\text{K}0} = 0.3M_{\text{ej}}v_{\text{sc}0}^2$ (see [Arnett 1982](#) and footnote 1 of [Wheeler et al. 2015](#)) and listed in Table 3. The initial rotational energy of the corresponding magnetars and the accumulative fraction (η) of the magnetars' rotational energy converted to the ejecta KE are also listed in Table 3.

Figure 5 shows the distributions of these best-fitting parameters (initial periods P_0 , magnetic strength B_p , ejecta masses M_{ej} , initial scale velocities $v_{\text{sc}0}$, and the gamma-ray opacity κ_{γ}), the derived parameter (initial KE $E_{\text{K}0}$), and the conversion fraction (η).

4. DISCUSSION

In our adopted model, the initial velocity of the SN ejecta is also a free parameter, rather than a measurable quantity. The magnetar wind would accelerate the ejecta, sweep up the material into a (thin) shell and produce a bubble between the center and the shell. We fit the observed photospheric velocities v_{ph} (even though they are always smaller than the scale velocities v_{sc}) and find the theoretical velocities of the ejecta of 6 SLSNe are in excellent agreement with the observations. However, we would point out that the velocity data of the remaining SLSNe in our sample cannot be well reproduced by the model.

In most of the previous studies, the KE E_{K} was a constant since the scale velocity v_{sc} is fixed to be a constant ($v_{\text{sc}} = v_{\text{sc}0}$), then the inferred KE is equivalent to the initial KE ($E_{\text{K}} = E_{\text{K}0}$). This assumption would cause two problems.

First, if we neglect the acceleration effect from the magnetar wind, the ejecta expansion is homologous ($v_{\text{sc}}(x) \propto x$, where x is the distance between the arbitrary point in the ejecta to the center), and the KE of the ejecta is $E_{\text{K}} = 0.3M_{\text{ej}}v_{\text{sc}}^2$. According to this formula, we find that the initial KEs of almost all SLSNe in the literature are $\gtrsim 5 \times 10^{51}$ erg if the acceleration effect is neglected. Most SLSNe might be CCSNe and their initial KE should be given by neutrinos coming from proto-neutron stars. The multi-dimensional sim-

ulations of neutrino-driven SNe find that the upper limit of the KE provided by neutrinos is $\sim 2.0 \times 10^{51}$ erg or $\sim 2.5 \times 10^{51}$ erg (Ugliano et al. 2012; Ertl et al. 2016; Müller et al. 2016; Sukhbold et al. 2016). Even if we adopt the looser upper limit ($\sim 2.5 \times 10^{51}$ erg), it is still significantly smaller than the inferred KE ($\gtrsim 5 \times 10^{51}$ erg) of the SLSNe. It seems evident that some other mechanisms are required to provide the additional initial KE.

To solve this problem, one might assume that the energy injection process must be divided into two steps: (1) the magnetar releases $\gtrsim 3 \times 10^{51}$ erg of the rotational energy at very short interval (“explosive injection”), and (2) the magnetar continuously injects its rotational energy to SN ejecta (“continuous injection”). As pointed out by Ioka et al. (2016), this two-step injection scenario needs an exotic behavior: the magnetic field should be initially large, resulting in a fast energy injection for a short duration, and then it may decay rapidly between the explosive injection and continuous injection.

Second, the initial rotational energy of a magnetar with an initial period P_0 is $\frac{1}{2}I\Omega_0^2 \simeq 2 \times 10^{52} (I/10^{45} \text{ g cm}^2) (P_0/1 \text{ ms})^{-2}$ erg. Here I is the moment of inertia of the magnetar and Ω_0 is its initial angular velocity. If $P_0 = 1 - 5$ ms, the initial rotational energy is $\simeq 1 - 20 \times 10^{51}$ erg. Calculations (Kasen & Bildsten 2010; Woosley 2010; Wang et al. 2017b) have indicated that a fraction of the initial rotational energy of a magnetar would be converted to the KE of SNe.⁷ This huge amount of energy and its acceleration effect cannot be neglected.

Our modelings based on the magnetar-powered model (Wang et al. 2017b) can simultaneously solve these two problems by taking into account the acceleration effect of the magnetar wind. We find that $\sim 19 - 97\%$ of the initial rotational energy of the magnetars have been converted to the KE of the ejecta (see Table 3 and Figure 6 for some of these SLSNe) and the initial KE of 15 SLSNe in our sample are smaller than 2.5×10^{51} erg (see Table 3) provided by the neutrino-driven mechanism for CCSNe. The additional KE is provided by the magnetar wind which accelerates the ejecta.

Besides, LSQ14mo, SN 2015bn and DES13S2cmm have initial KE (slightly) larger than $\sim 2.5 \times 10^{51}$ erg but the initial KE of these SLSNe can be halved to be $\sim 1.37 \times 10^{51}$, $\sim 1.41 \times 10^{51}$, and $\sim 2.28 \times 10^{51}$ erg if the value of κ doubled ($\kappa = 0.2 \text{ cm}^{-2} \text{ g}^{-1}$) so that their ejecta masses can be halved. Therefore, these three SLSNe can also be explained by the magnetar model. The only SLSN whose KE cannot be explained by the magnetar-powered model is DES14X3taz since its initial KE is 4.51×10^{52} erg (if $\kappa = 0.1 \text{ cm}^{-2} \text{ g}^{-1}$) or 2.25×10^{52} erg (if $\kappa = 0.2 \text{ cm}^{-2} \text{ g}^{-1}$), significantly larger than that can be provided by the neutrinos.

All in all, in our model, the neutrinos provide the initial KE of the ejecta, and the magnetar accelerates the ejecta so that they have large final KE ($\gtrsim 5 \times 10^{51}$ erg). Thus the difficulty of explaining the origin of the KE of the SLSNe can be solved by taking into account the

acceleration effect.⁸

Figure 7 shows the conversion fraction η versus magnetic strength B_p . The correlation coefficient between these two quantities is $R = 0.715$, which means larger B_p results in a larger η . Wang et al. (2016c) demonstrated that the conversion fraction η is high if the spin-down timescale of the magnetar is short compared to the diffusion timescale. It is therefore expected that the stronger B_p , the higher η tends to be, although the other factors, e.g. M_{ej} , P_0 , will cause some scatters in this relation. If B_p is increased further to $\sim 10^{16}$ G, we can expect that most of the magnetar’s rotational energy will be converted to ejecta’s KE and the SNe will become dimmer. This is precisely what is seen for broad-lined type Ic SNe (SNe Ic-BL) by Wang et al. (2016b), who showed evidence that SNe Ic-BL 1998bw and 2002ap were powered by magnetars (Wang et al. 2017b). This implies a continuous spectrum of magnetar-powered SNe.

The inferred gamma-ray opacity κ_γ is $\sim 0.01 - 0.82 \text{ cm}^{-2} \text{ g}^{-1}$. Kotera et al. (2013) has demonstrated that the values of κ_γ must be between approximately 0.01 and $0.2 \text{ cm}^2 \text{ g}^{-1}$ if the emission is dominated by gamma photons, and between approximately 0.2 and $10^4 \text{ cm}^2 \text{ g}^{-1}$ if the emission is dominated by X-ray photons. In our sample, the values of κ_γ of PTF12dam and SSS 120810 reach the lower limit, $\sim 0.01 \text{ cm}^2 \text{ g}^{-1}$, proposed by the theoretical prediction (see also Chen et al. 2015 for PTF12dam), suggesting that the energy of the gamma-ray radiation from the magnetars associated with these SLSNe must be higher than $3 \times 10^7 \text{ eV} = 30 \text{ MeV}$. Such high-energy photons from magnetars have already been observed (Hester 2008; Bühler & Blandford 2014) and can be explained by theoretical modelings (Metzger et al. 2014; Murase et al. 2015; Wang et al. 2016a).

For SLSNe in Figure 2, bolometric luminosity (L) and temperature (T) evolution can be well fitted but the evolution of photospheric velocity (v_{ph}) cannot be fitted. This is strange since $L = 4\pi\sigma T^4 R_{\text{ph}}^2 = 4\pi\sigma T^4 (\int_{v_{\text{ph}0}}^{v_{\text{ph}}} v_{\text{ph}} dt)^2$ ($R_{\text{ph}} = \int_{v_{\text{ph}0}}^{v_{\text{ph}}} v_{\text{ph}} dt$ is the photospheric radius). The reason for this might be that the error bars of the observational data are too small. Observationally, the velocities inferred from different elements are rather different (e.g., see Figure 7 of Taddia et al. 2016), so the error bars of the velocity data might be larger than that presented in the Figure 2. To clarify this issue, more dedicated studies are required.

Some of the SLSNe in Figure 3 show flattening (SN 2011ke, SN 2015bn, PS1-11ap, PS1-14bj) in the late-time temperature evolution. This flattening may be caused by recombination, which is not considered in our adopted model. The most extreme case is PS1-14bj, whose temperature evolution is rather flat at very beginning, and even slightly increasing with time. Another peculiar case is DES14X3taz, whose temperature evolution is untypical in the SN sample. We note that the SLSNe mentioned above (PS1-14bj, SN 2015bn and DES14X3taz) are among the four SLSNe that are not well fitted by our model. These peculiar SLSNe deserve more investi-

⁷ For example, Woosley (2010) demonstrated that a magnetar with $P_0 = 4.5$ ms and $B_p = 1 \times 10^{14}$ G would convert 40% of its initial rotational energy to the KE of the SN ejecta.

⁸ The models proposed by Kasen & Bildsten (2010) and Woosley (2010) also took into account the acceleration effect and can also solve the problem associated with the initial KE. However, these models neglected the leakage effect.

gations. The large reduced χ^2 of SN 2013dg (among the four largest reduced χ^2), on the other hand, is caused by the small errors in temperature measurement because its light-curve and velocity fitting quality is similar to PTF11rks.

5. CONCLUSIONS

Detailed studies of SLSNe in the last decade have revealed many important observational properties and given some crucial clues to understanding the energy-source models and the explosion mechanisms of SLSNe. In the last several years, most SLSNe discovered are type I whose light curves and spectra are diverse and complex (e.g., [Inserra et al. 2017](#)).

Using the magnetar-powered model and the MCMC approach, we fit the light curves, temperature evolution, and photospheric velocity evolution of 19 SLSNe I. We get rather good fits for 7 events ($\chi^2/\text{d.o.f} = 0.24 - 0.96$) and good fits for other 7 events ($\chi^2/\text{d.o.f} = 1.37 - 3.13$), suggesting that these SLSNe can be explained by the magnetar model. Four events cannot be well fitted by this model ($\chi^2/\text{d.o.f} = 4.32 - 6.83$), suggesting that these four events must be further studied.

The parameters determined by the MCMC code are as follows. The values of the initial period of the magnetars supposed to power these SLSNe are 1.2 – 8.3 ms; the values of the magnetic strength of the magnetars are $0.2 - 8.8 \times 10^{14}$ G; the masses of the ejecta of these SLSNe are $1 - 27.6 M_{\odot}$; the gamma-ray opacity are 0.01 – 0.82 $\text{cm}^2 \text{g}^{-1}$.

More importantly, we take into account the acceleration effect and let the initial velocity of the ejecta be a free parameter and find that the initial KE of most SLSNe in our sample are (significantly) smaller than the upper limit ($\sim 2.5 \times 10^{51}$ erg) of the KE provided by

the neutrino-driven mechanism for CCSNe, indicating that our modelings are self-consistent and do not need any exotic assumption (e.g., two-step injections from the magnetars) to explain the origin of the ejecta kinetic energy of these SLSNe.

Our modeling shows that $\sim 19 - 97\%$ of the initial rotational energy of the magnetars is converted to the KE of the SNe ejecta. This acceleration effect is especially important in the SLSNe that require magnetars with initial periods $P_0 \sim 1 - 5$ ms, since the initial rotational energy of these magnetars is $\sim 1 - 20 \times 10^{51}$ erg and would convert $\sim 0.2 - 20 \times 10^{51}$ erg to KE of the SLSNe ejecta.

By combining these two results, we demonstrate that the KE acquired from the rotational energy dissipated via magnetic dipole radiation can naturally provide a considerable amount of the KE for the SN ejecta, and the difficulty of explaining the KE of the SLSNe whose KE are usually (significantly) larger than 2×10^{51} erg can be solved.

Understanding the nature of SLSNe is one of the most challenging questions in astrophysics. Their explosion mechanisms and energy sources are still ambiguous. Our results provide some new and important clues related to these problems. To clarify these important issues, more observations and theoretical work are needed to be done.

We thank the referee for very constructive suggestions which have allowed us to improve this manuscript significantly. This work was supported by the National Basic Research Program (“973” Program) of China (grant no. 2014CB845800) and the National Natural Science Foundation of China (grants no. 11573014, U1331202, 11533033, 11422325, 11373022, and 11673006).

REFERENCES

- Arnett, W. D. 1982, *ApJ*, 253, 785
 Barkat, Z., Rakavy, G., & Sack, N. 1967, *Phys. Rev. Lett.*, 18, 379
 Bühler, R., & Blandford, R. 2014, *RPPh*, 77, 066901
 Chatzopoulos, E., Wheeler, J. C., & Vinko, J. 2012, *ApJ*, 746, 121
 Chen, T.-W., Smartt, S. J., Jerkstrand, A., et al. 2015, *MNRAS*, 452, 1567
 Chen, T.-W., Nicholl, M., Smartt, S. J., et al. 2016, *A&A*, in press (arXiv:1611.09910)
 Chevalier, R. A. 1982, *ApJ*, 258, 790
 Chevalier, R. A., & Fransson, C. 1994, *ApJ*, 420, 268
 Chevalier, R. A., & Irwin, C. M. 2011, *ApJL*, 729, L6
 Chugai, N. N. 2009, *MNRAS*, 400, 866
 Chugai, N. N., & Danziger, I. J. 1994, *MNRAS*, 268, 173
 Chomiuk, L., Chornock, R., Soderberg, A. M., et al. 2011, *ApJ*, 743, 114
 Colgate, S. A., & McKee, C. 1969, *ApJ*, 157, 623
 Colgate, S. A., Petschek, A. G., & Kriese, J. T. 1980, *ApJL*, 237, L81
 Cooke, J., Sullivan, M., Gal-Yam, A., et al. 2012, *Nature*, 491, 228
 Dai, Z. G., Wang, S. Q., Wang, J. S., Wang, L. J., & Yu, Y. W. 2016, *ApJ*, 817, 132
 Dessart, L., Hillier, D. J., Waldman, R., Livne, E., & Blondin, S. 2012, *MNRAS*, 426, L76
 Ertl, T., Janka, H.-T., Woosley, S. E., Sukhbold, T., & Ugliano, M. 2016, *ApJ*, 818, 124
 Filippenko, A. V. 1997, *ARA&A*, 35, 309
 Gal-Yam, A., Mazzali, P., Ofek, E. O., et al. 2009, *Nature*, 462, 624
 Gal-Yam, A. 2012, *Science*, 337, 927
 Gal-Yam, A. 2016, arXiv:1611.09353
 Gezari, S., Halpern, J. P., Grupe, D., et al. 2009, *ApJ*, 690, 1313
 Ginzburg, S., & Balberg, S. 2012, *ApJ*, 757, 178
 Hester, J. J. 2008, *ARA&A*, 46, 127
 Inserra, C., Smartt, S. J., Jerkstrand, A., et al. 2013, *ApJ*, 770, 128
 Inserra, C., Smartt, S. J., Gall, E. E. E., et al. 2016, arXiv:1604.01226
 Inserra, C., Nicholl, M., Chen, T.-W., et al. 2017, *MNRAS*, in press (arXiv: 1701.00941)
 Ioka, K., Hotokezaka, K., & Piran, T. 2016, *ApJ*, 833, 110
 Janka, H.-T., Melson, T., & Summa, A. 2016, *ARNPS*, 66, 341
 Kangas, T., Blagorodnova, N., Mattila, S., et al. 2016, arXiv:1611.10207
 Kasen, D., & Bildsten, L. 2010, *ApJ*, 717, 245
 Kotera, K., Phinney, E. S., & Olinto, A. V. 2013, *MNRAS*, 432, 3228
 Lunnan, R., Chornock, R., Berger, E., et al. 2013, *ApJ*, 771, 97
 Lunnan, R., Chornock, R., Berger, E., et al. 2016, *ApJ*, 831, 144
 Maeda, K., Tanaka, M., Nomoto, K., et al. 2007, *ApJ*, 666, 1069
 Mazzali, P. A., Walker, E. S., Pian, E., et al. 2013, *MNRAS*, 432, 2463
 Metzger, B. D., Vurm, I., Hascoët, R., & Beloborodov, A. M. 2014, *MNRAS*, 437, 703
 McCrum, M., Smartt, S. J., Kotak, R., et al. 2014, *MNRAS*, 437, 656
 Miller, A. A., Chornock, R., Perley, D.A., et al. 2009, *ApJ*, 690, 1303
 Moriya, T. J., Blinnikov, S. I., Tominaga, N., Yoshida, N., Tanaka, M., Maeda, K., & Nomoto, K. 2013, *MNRAS*, 428, 1020
 Müller, B., Heger, A., Liptai, D., & Cameron, J. B. 2016, *MNRAS*, 460, 742

- Murase, K., Kashiyama, K., Kiuchi, K., & Bartos, I. 2015, *ApJ*, 805, 82
- Nicholl, M., Smartt, S. J., Jerkstrand, A., et al. 2013, *Nature*, 502, 346
- Nicholl, M., Jerkstrand, A., Inserra, C., et al. 2014, *MNRAS*, 444, 2096
- Nicholl, M., Smartt, S. J., Jerkstrand, A., et al. 2015a, *ApJL*, 807, L18
- Nicholl, M., Smartt, S. J., Jerkstrand, A., et al. 2015b, *MNRAS*, 452, 3869
- Nicholl, M. & Smartt, S. J. 2016, *MNRAS*, 457, 79
- Nicholl, M., Berger, E., Smartt, S. J., et al. 2016a, *ApJ*, 826, 39
- Nicholl, M., Berger, E., Margutti, R., et al. 2016b, *ApJL*, 828, L18
- Ostriker, J. P., & Gunn, J. E. 1971, *ApJL*, 164, L95
- Papadopoulos, A., D'Andrea, C. B., Sullivan, M., et al. 2015, *MNRAS*, 449, 1215
- Pastorello, A., Smartt, S. J., Botticella, M. T., et al. 2010, *ApJL*, 724, L16
- Quimby, R. M., Kulkarni, S. R., Kasliwal, M. M., et al. 2011, *Nature*, 474, 487
- Quimby, R. M., Werner, M. C., Oguri, M., et al. 2011, *ApJ*, 768, 20
- Quimby, R. M., Oguri, M., More, A., et al. 2014, *Science*, 344, 396
- Rakavy, G., & Shaviv, G. 1967, *ApJ*, 148, 803
- Shapiro, S. L., & Teukolsky, S. A. 1983, *Black Holes, White Dwarfs, and Neutron Stars: The Physics of Compact Objects* (New York: Wiley)
- Smith, N., & McCray, R. 2007, *ApJL*, 671, L17
- Smith, M., Sullivan, M., D'Andrea, C. B., et al. 2016, *ApJL*, 818, L8
- Sukhbold, T., Ertl, T., Woosley, S. E., Brown, J. M., & Janka, H.-T. 2016, *ApJ*, 821, 38
- Taddia, F., Fremling, C., Sollerman, J., et al. 2016, *A&A*, 592, 89
- Ugliano, M., Janka, H.-T., Marek, A., et al. 2012, *ApJ*, 757, 69
- Vreeswijk, P. M., Leloudas, G., Gal-Yam, A., et al. 2017, *ApJ*, 835, 58
- Wang, L. J., Cano, Z., Wang, S. Q., et al. 2017a, *ApJ*, submitted (arXiv:1702.03156)
- Wang, L. J., Dai, Z. G., Liu, L. D., & Wu, X. F. 2016a, *ApJ*, 823, 15
- Wang, L. J., Han, Y. H., Xu, D., et al. 2016b, *ApJ*, 831, 41
- Wang, L. J., Wang, S. Q., Dai, Z. G., Xu, D., Han, Y. H., Wu, X. F., & Wei, J. Y. 2016c, *ApJ*, 821, 22
- Wang, L. J., Yu, H., Liu, L. D., Wang, S. Q., Han, Y. H., Xu, D., Dai, Z. G., Qiu, Y. L., & Wei, J. Y. 2017b, *ApJ*, 837, 128
- Wang, S. Q., Liu, L. D., Dai, Z. G., Wang, L. J., & Wu, X. F. 2016d, *ApJ*, 828, 87
- Wang, S. Q., Wang, L. J., Dai, Z. G., & Wu, X. F. 2015a, *ApJ*, 799, 107
- Wang, S. Q., Wang, L. J., Dai, Z. G., & Wu, X. F. 2015b, *ApJ*, 807, 147
- Wheeler, J. C., Johnson, V., & Clacchiatti, A. 2015, *MNRAS*, 450, 1295
- Woosley, S. E. 2010, *ApJL*, 719, L204

TABLE 1
SLSNe IN OUR SAMPLE

SN name	Redshift (z)	Peak Luminosity (10^{44} erg s^{-1})	Reference
DES13S2cmm	0.663	0.63	(Papadopoulos et al. 2015)
DES14X3taz	0.608	2.20	(Smith et al. 2016)
Gaia16apd	0.102	3.01	(Kangas et al. 2016)
LSQ12dlf	0.25	1.03	(Nicholl et al. 2014)
LSQ14mo	0.256	1.09	(Chen et al. 2016)
PS1-10awh	0.908	2.41	(Chomiuk et al. 2011)
PS1-10bzj	0.65	1.07	(Lunnan et al. 2013)
PS1-11ap	0.524	0.72	(McCrum et al. 2014)
PS1-14bj	0.521	0.46	(Lunnan et al. 2016)
PTF10hgi	0.099	0.35	(Inserra et al. 2013)
PTF11rks	0.193	0.47	(Inserra et al. 2013)
PTF12dam	0.108	1.17	(Nicholl et al. 2013)
SN 2010gx	0.231	0.91	(Inserra et al. 2013)
SN 2011ke	0.143	0.81	(Inserra et al. 2013)
SN 2011kf	0.245	3.72	(Inserra et al. 2013)
SN 2012il	0.175	0.80	(Inserra et al. 2013)
SN 2013dg	0.26	0.74	(Nicholl et al. 2014)
SN 2015bn	0.114	2.42	(Nicholl et al. 2016a)
SSS 120810	0.17	1.04	(Nicholl et al. 2014)

TABLE 2
BEST-FIT PARAMETERS FOR OUR SAMPLE OF SLSNE.

SN name	P_0 (ms)	B_p (10^{14} G)	M_{ej} (M_\odot)	κ_γ ($\text{cm}^2 \text{g}^{-1}$)	v_{sc0} (km s^{-1})	T_{start} (days)	χ^2/dof
DES13S2cmm	5.5 ^{+0.07} _{-0.07}	1.8 ^{+0.14} _{-0.13}	7.2 ^{+1.14} _{-0.94}	0.33 ^{+0.18} _{-0.18}	10286 ⁺⁴⁹³ ₋₄₅₃	-33.0 ^{+1.1} _{-1.1}	3.12
DES14X3taz	1.3 ^{+0.20} _{-0.28}	0.2 ^{+0.08} _{-0.05}	24.5 ^{+4.83} _{-3.60}	≤ 0.06	17517 ⁺¹²⁶⁷ ₋₁₂₁₃	-40.1 ^{+1.2} _{-1.0}	4.32
Gaia16apd	2.1 ^{+0.18} _{-0.13}	2.2 ^{+0.13} _{-0.10}	3.2 ^{+0.21} _{-0.20}	0.57 ^{+0.21} _{-0.32}	8618 ⁺¹⁰⁰² ₋₁₂₀₄	-35.9 ^{+0.9} _{-0.6}	0.64
LSQ12dlf	1.3 ^{+0.33} _{-0.09}	5.5 ^{+0.14} _{-0.23}	14.5 ^{+1.20} _{-1.31}	0.23 ^{+0.20} _{-0.18}	≤ 2226	-21.2 ^{+0.4} _{-0.6}	3.13
LSQ14mo	3.0 ^{+0.76} _{-0.82}	6.9 ^{+0.68} _{-3.89}	6.8 ^{+2.59} _{-0.62}	0.26 ^{+0.19} _{-0.17}	8192 ⁺¹⁹⁵⁹ ₋₁₉₂₉	-21.1 ^{+0.9} _{-6.6}	0.40
PS1-10awh	2.5 ^{+1.15} _{-1.01}	0.5 ^{+1.17} _{-0.36}	1.0 ^{+0.39} _{-0.39}	0.10 ^{+0.07} _{-0.07}	13383 ⁺⁴²⁷ ₋₄₂₅	-24.8 ^{+0.5} _{-0.5}	0.44
PS1-10bzj	1.2 ^{+0.41} _{-0.24}	7.8 ^{+0.40} _{-0.49}	12.2 ^{+3.35} _{-2.45}	0.30 ^{+0.20} _{-0.20}	1740 ⁺¹⁷³⁵ ₋₁₄₇₈	-18.6 ^{+0.3} _{-0.5}	0.24
PS1-11ap	3.9 ^{+0.09} _{-0.08}	2.1 ^{+0.06} _{-0.06}	6.1 ^{+0.46} _{-0.40}	0.22 ^{+0.25} _{-0.15}	≤ 3536	-48.6 ^{+0.9} _{-0.9}	0.53
PS1-14bj	2.7 ^{+0.16} _{-0.14}	0.4 ^{+0.08} _{-0.06}	27.6 ^{+2.81} _{-2.71}	≤ 0.08	1158 ⁺⁴⁵⁰ ₋₅₉₄	-172.6 ^{+6.4} _{-6.4}	6.83
PTF10hgi	8.3 ^{+0.22} _{-0.25}	3.0 ^{+0.16} _{-0.17}	1.2 ^{+0.38} _{-0.16}	0.19 ^{+0.21} _{-0.09}	≤ 4112	-5.3 ^{+1.9} _{-2.2}	1.37
PTF11rks	6.9 ^{+0.68} _{-0.89}	8.8 ^{+1.04} _{-0.87}	3.5 ^{+0.57} _{-0.49}	≥ 0.15	8044 ⁺⁵⁷⁶ ₋₅₇₄	1.3 ^{+0.5} _{-0.5}	2.94
PTF12dam	2.7 ^{+0.10} _{-0.13}	0.8 ^{+0.17} _{-0.20}	12.0 ^{+3.48} _{-2.55}	0.01 ^{+0.006} _{-0.005}	≤ 2345	-69.9 ^{+3.1} _{-3.6}	0.39
SN 2010gx	1.3 ^{+1.07} _{-0.20}	8.5 ^{+0.38} _{-1.18}	12.8 ^{+1.28} _{-1.29}	0.04 ^{+0.24} _{-0.02}	4233 ⁺⁴⁴³⁸ ₋₃₉₀₂	-1.8 ^{+0.8} _{-1.0}	0.96
SN 2011ke	2.6 ^{+0.22} _{-0.17}	7.1 ^{+0.15} _{-0.15}	6.4 ^{+0.50} _{-0.47}	0.71 ^{+0.20} _{-0.24}	1816 ⁺²²⁷⁰ ₋₁₀₄₅	9.7 ^{+0.5} _{-0.6}	3.46
SN 2011kf	2.1 ^{+0.16} _{-0.15}	5.2 ^{+0.11} _{-0.12}	2.1 ^{+0.16} _{-0.15}	0.82 ^{+0.12} _{-0.14}	≤ 3704	0.5 ^{+0.4} _{-0.5}	1.91
SN 2012il	5.9 ^{+0.15} _{-0.15}	4.6 ^{+0.05} _{-0.05}	1.6 ^{+0.15} _{-0.15}	≥ 0.4	≤ 3595	-2.3 ^{+0.6} _{-0.7}	2.47
SN 2013dg	4.4 ^{+0.59} _{-0.67}	1.2 ^{+0.53} _{-0.36}	1.2 ^{+0.31} _{-0.27}	≥ 0.15	≤ 4072	-30.5 ^{+1.4} _{-1.1}	5.52
SN 2015bn	2.3 ^{+0.05} _{-0.10}	0.5 ^{+0.03} _{-0.05}	10.1 ^{+0.37} _{-0.20}	0.03 ^{+0.008} _{-0.007}	6798 ⁺¹⁵⁰ ₋₁₁₃	-65.1 ^{+1.1} _{-1.5}	6.15
SSS 120810	2.5 ^{+0.27} _{-0.22}	3.7 ^{+0.19} _{-0.22}	2.9 ^{+1.45} _{-1.42}	0.01 ^{+0.007} _{-0.006}	10961 ⁺¹⁷²⁸ ₋₂₄₃₅	-30.2 ^{+0.2} _{-0.4}	1.76

Note. The uncertainties are 1σ errors.

TABLE 3
DERIVED PHYSICAL PARAMETERS

SN name	E_{K0}^a (10^{51} erg)	E_{p0}^b (10^{51} erg)	η^c	(P_0, B_p) (ms, 10^{14} G)
DES13S2cmm	4.55	0.65	0.89	(5.5, 1.8)
DES14X3taz	45.1	11.8	0.27	(1.3, 0.2)
Gaia16apd	1.99	3.77	0.46	(2.1, 2.2)
LSQ12dlf	0.1–0.43	10.92	0.97	(1.3, 5.5)
LSQ14mo	2.74	2.14	0.86	(3.0, 6.9)
PS1-10awh	1.08	3.15	0.39	(2.5, 0.5)
PS1-10bzj	0.22	13.25	0.97	(1.2, 7.8)
PS1-11ap	0.1–0.45	1.30	0.53	(3.9, 2.1)
PS1-14bj	0.22	2.81	0.23	(2.7, 0.4)
PTF10hgi	0.1–0.12	0.28	0.27	(8.3, 3.0)
PTF11rks	1.37	0.42	0.68	(6.9, 8.8)
PTF12dam	0.1–0.39	2.76	0.38	(2.7, 0.8)
SN 2010gx	1.38	11.82	0.97	(1.3, 8.5)
SN 2011ke	0.13	2.92	0.90	(2.6, 7.1)
SN 2011kf	0.1–0.17	4.49	0.80	(2.1, 5.2)
SN 2012il	0.1–0.12	0.57	0.52	(5.9, 4.6)
SN 2013dg	0.1–0.12	1.03	0.19	(4.4, 1.2)
SN 2015bn	2.80	3.87	0.20	(2.3, 0.5)
SSS120810	2.12	3.24	0.83	(2.5, 3.7)

- a. E_{K0} is the initial kinetic energy of the SLSNe and its lower-limit has been set to be 1×10^{50} erg.
b. $E_{p0} \simeq 2 \times 10^{52} (P_0/1 \text{ ms})^{-2}$ erg is the initial rotational energy of the magnetars proposed to power the SLSNe.
c. η is the accumulative fraction of the rotational energy of the magnetar converted to the kinetic energy of these SLSNe.

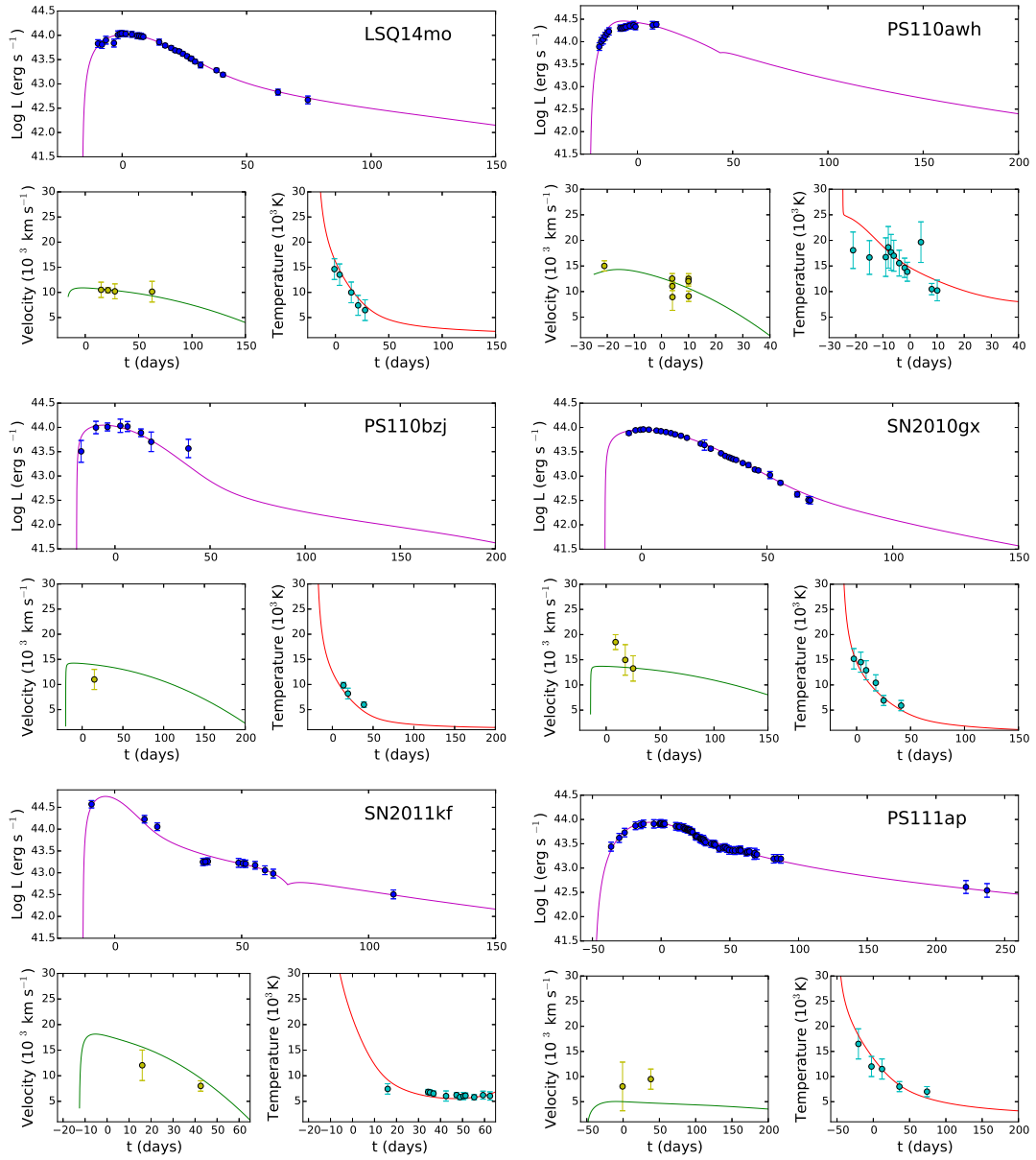


FIG. 1.— Model fits for light curves, temperature evolution, and velocity evolution of LSQ14mo, PS1-10awh, PS1-10bjz, SN 2010gx, SN 2011kf, and PS1-11ap. Parameters are shown in Table 2.

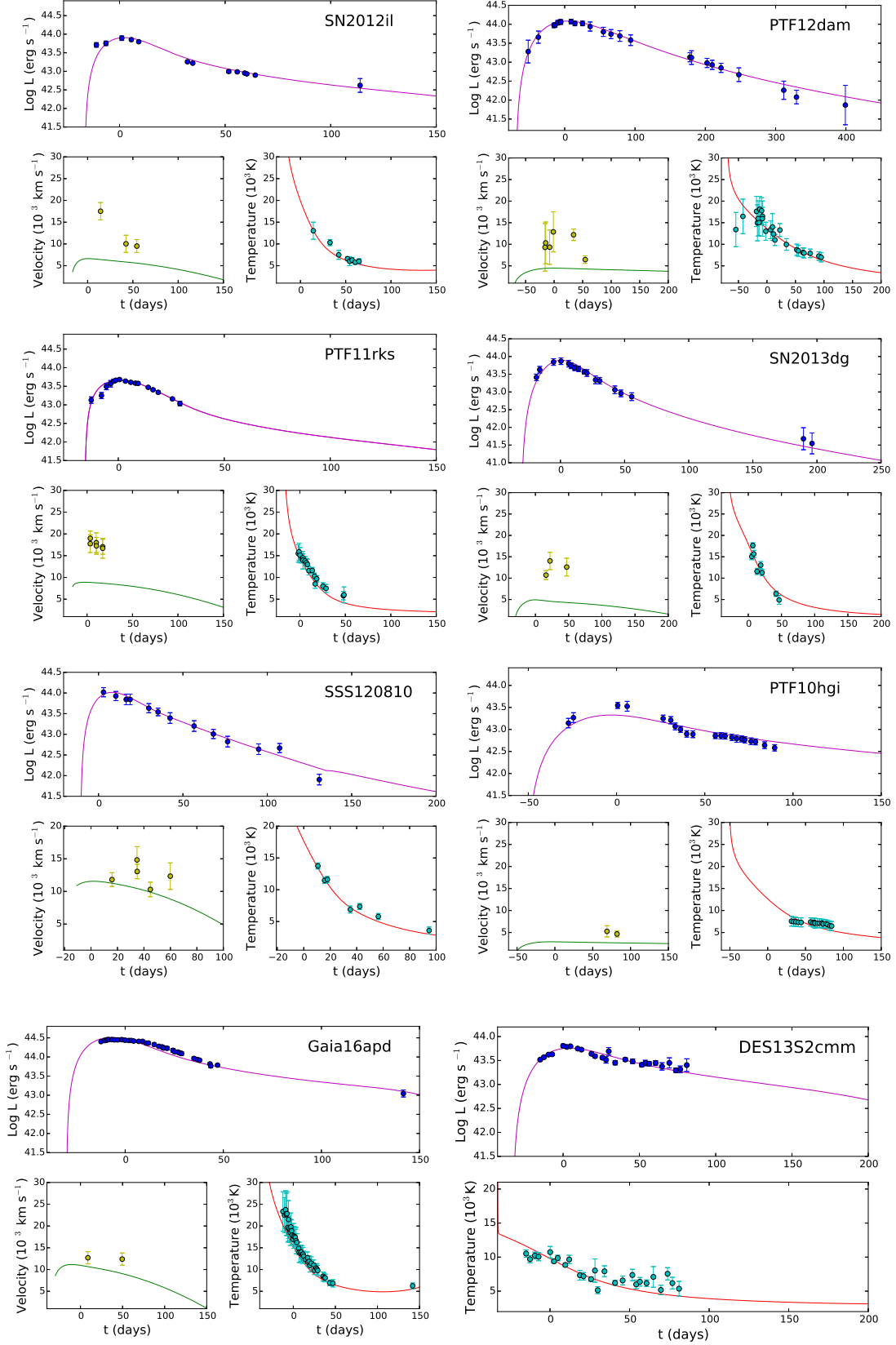


FIG. 2.— Model fits for light curves, temperature evolution, and velocity evolution of SN 2012il, PTF12dam, PTF11rks, SN 2013dg, SSS120810, PTF10hgi, Gaia16apd, and DES13S2cmm. Parameters are shown in Table 2.

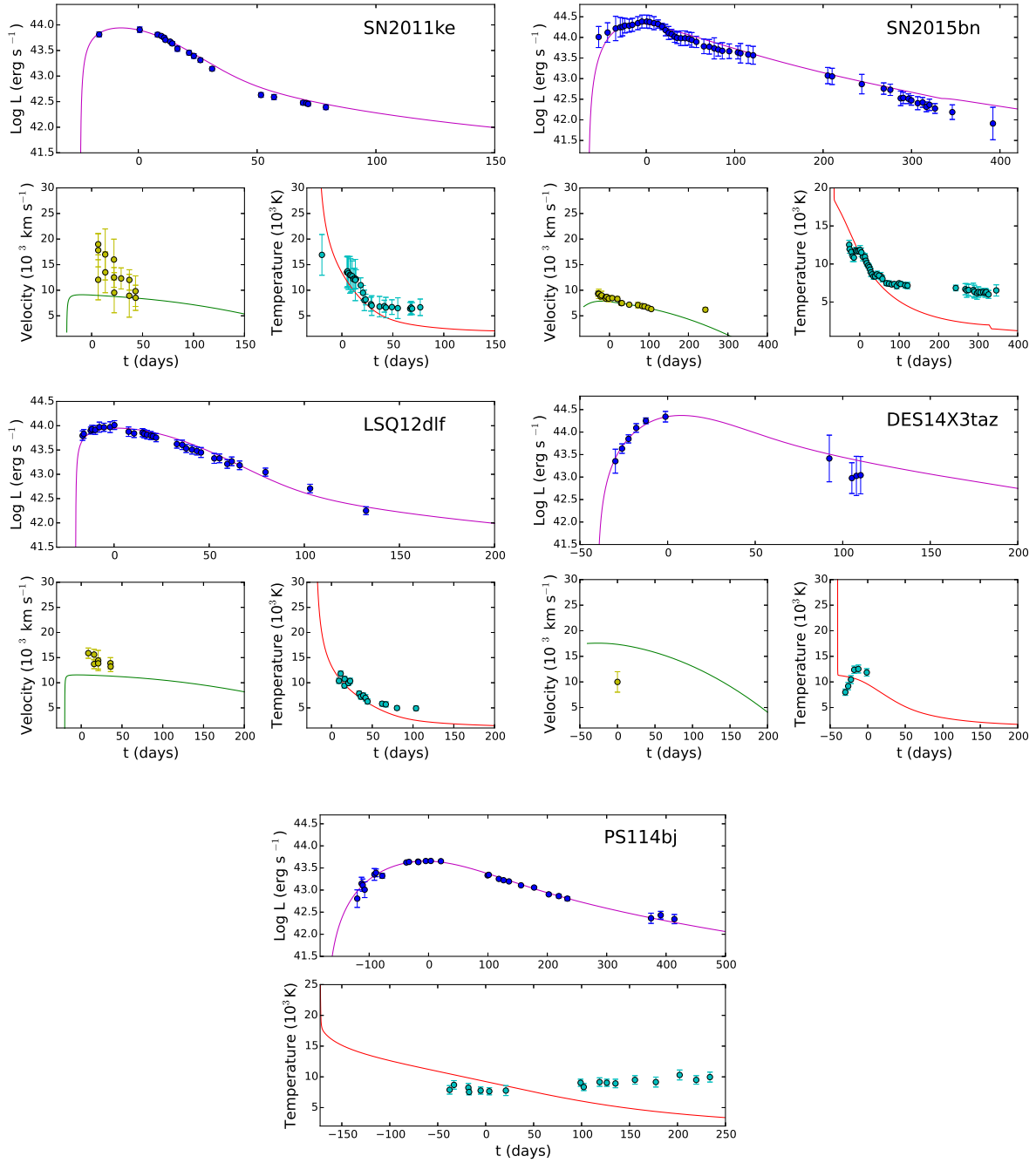


FIG. 3.— Model fits for light curves, temperature evolution, and velocity evolution of SN 2011ke, SN 2015bn, LSQ12dlf, DES14X3taz, and PS1-14bj. Parameters are shown in Table 2.

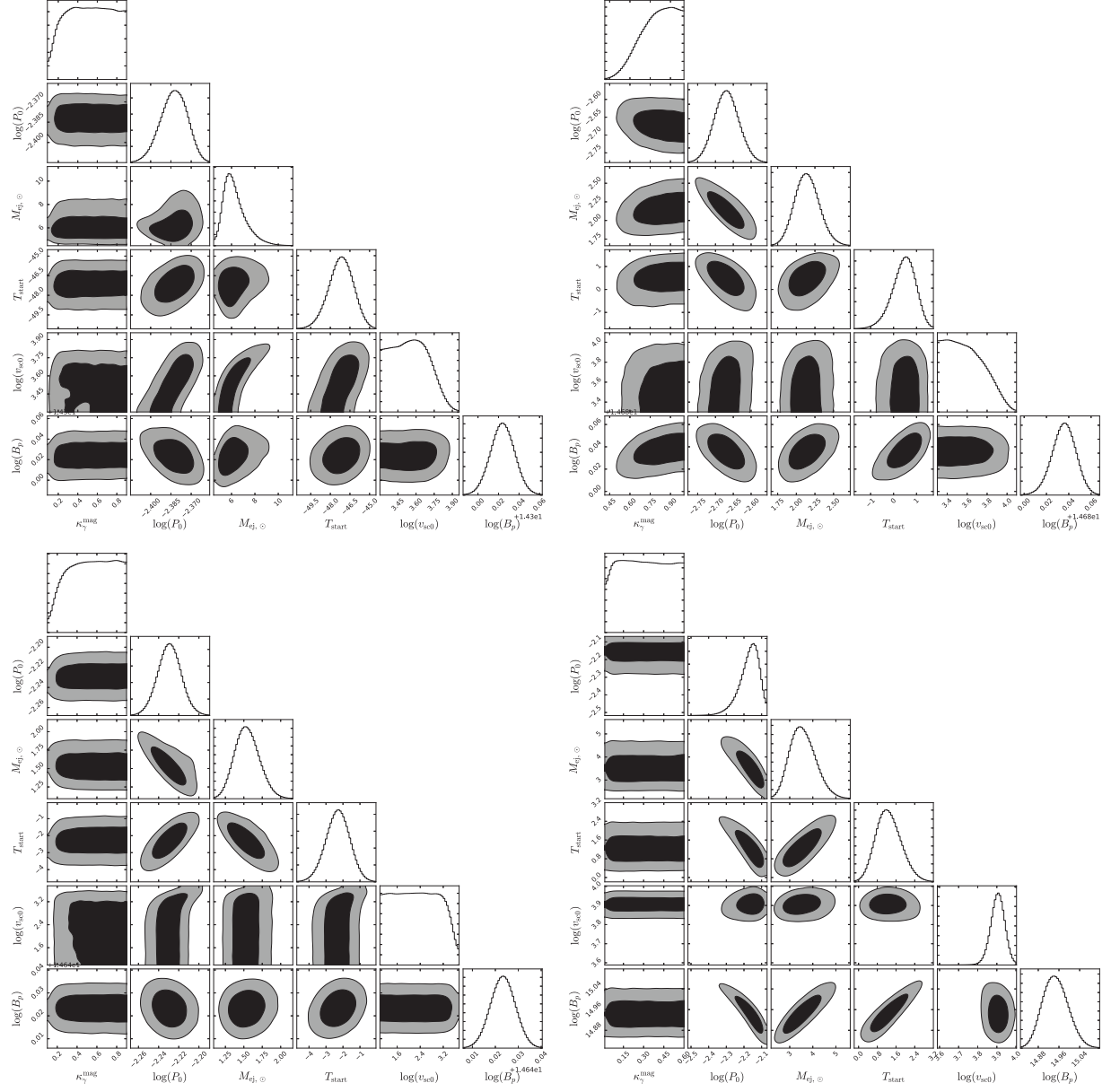


FIG. 4.— Confidence contours of parameter corner in the modeling of PS1-11ap, SN 2011kf, SN2012il and PTF11rks. The contours are 1 σ and 2 σ uncertainties, respectively.

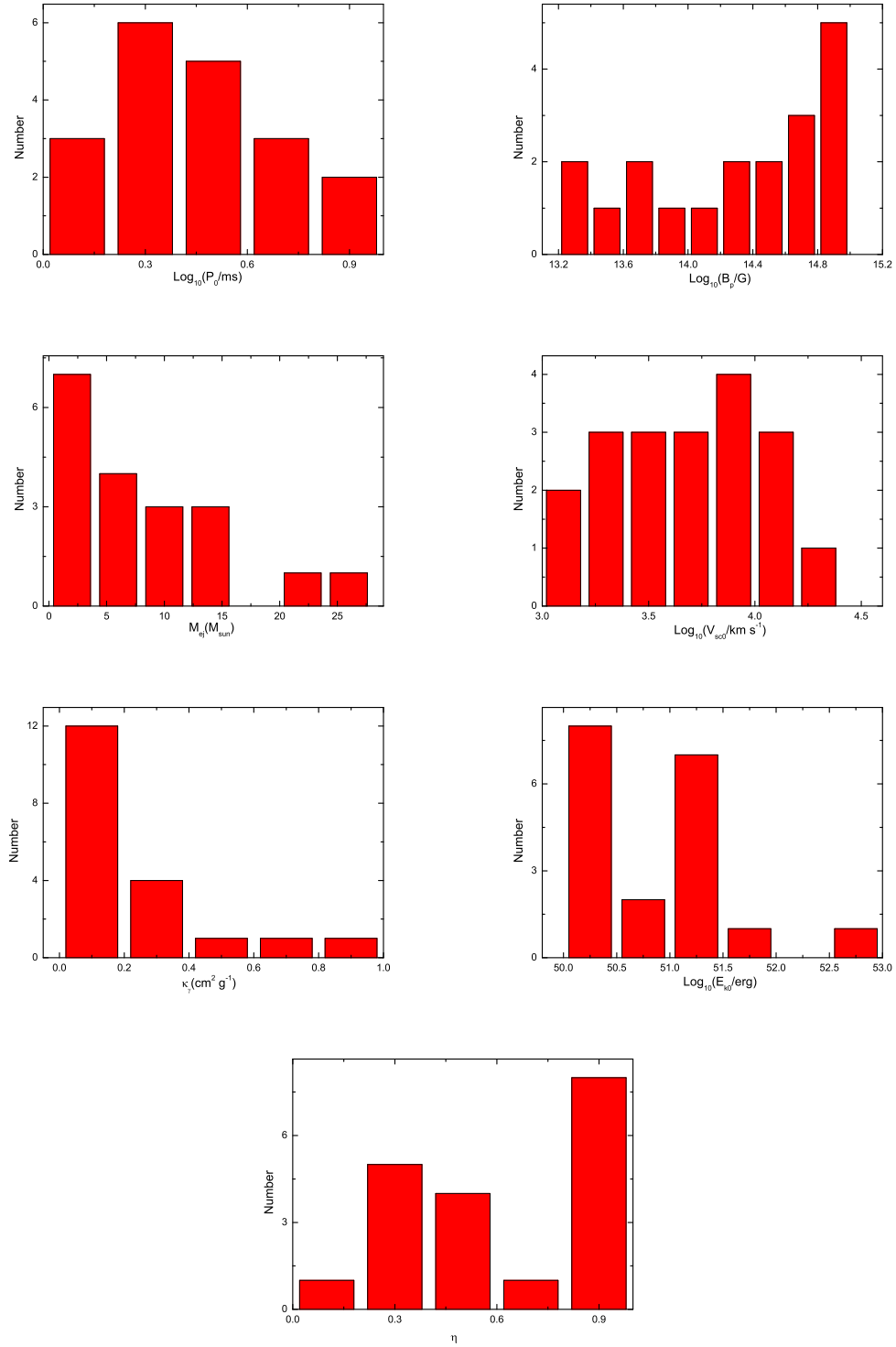


FIG. 5.— Distributions of the initial stellar periods P_0 , magnetic strength B_p , ejecta masses M_{ej} , initial scale velocities of the ejecta v_{sc0} , the gamma-ray opacity κ_{γ} , initial kinetic energy of the ejecta E_{K0} as well as the accumulative fraction of the rotational energy of the magnetar converted to the kinetic energy η in the modeling of the sample.

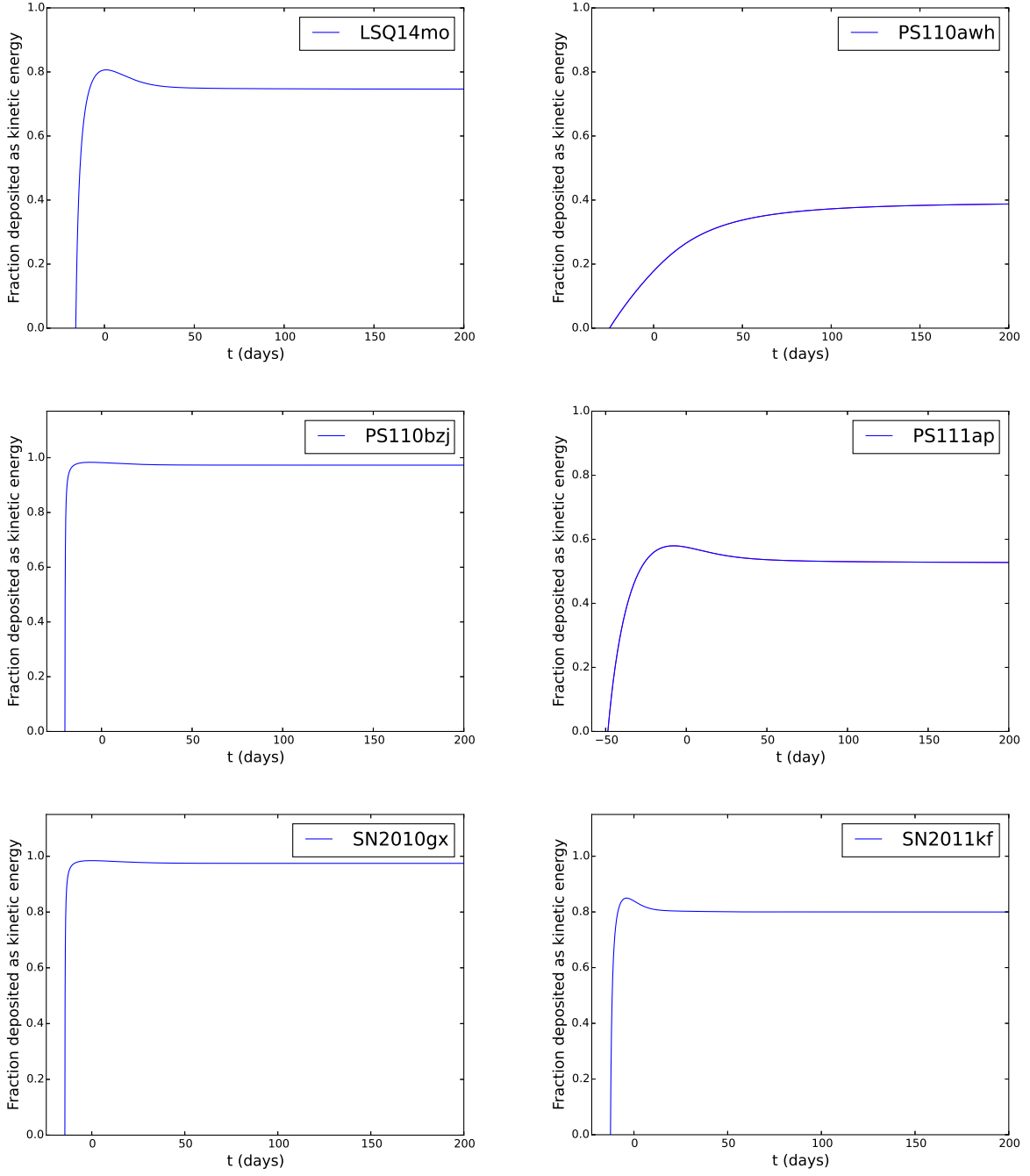


FIG. 6.— The accumulative fraction of the stellar rotational energy converted to the kinetic energy of LSQ14mo, PS1-10awh, PS1-10bzj, PS1-11ap, SN 2010gx, and SN 2011kf.

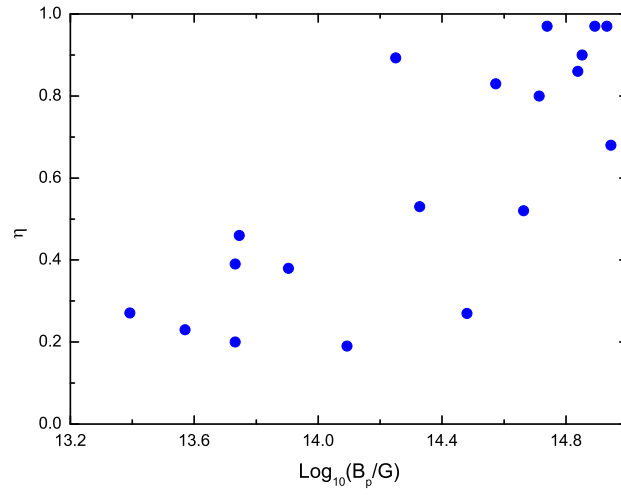


FIG. 7.— The magnetic strength (B_p) versus the final fraction (η) of the magnetar’s rotational energy converted to the kinetic energy. Parameters are listed in Table 3.